PCCP

PAPER

View Article Online
View Journal | View Issue

Cite this: *Phys. Chem. Chem. Phys.*, 2017, **19**, 24357

Insights into the mechanism of the capture of CO_2 by K_2CO_3 sorbent: a DFT study†

Hongyan Liu,[ab] Qiaoyun Qin,[a] Riguang Zhang,[a] Lixia Ling[ac] and Baojun Wang *[a]

Received 20th April 2017,
Accepted 4th August 2017

DOI: 10.1039/c7cp02579c

rsc.li/pccp

The adsorption and reactions of CO_2 and H_2O on both monoclinic and hexagonal crystal K_2CO_3 were investigated using the density functional theory (DFT) approach. The calculated adsorption energies showed that adsorption of H_2O molecules was clearly substantially stronger on the K_2CO_3 surface than the adsorption of CO_2, except on the (001)-1 surface of hexagonal K_2CO_3, where CO_2 is competitively adsorbed with H_2O. Carbonation reactions easily occur on pure K_2CO_3 and involve two parallel paths: one is where adsorbed H_2O reacts with molecular CO_2 in gas to form the bicarbonate, while the other is where H_2O dissociates into OH and H before bicarbonate formation, and then OH reacts with gaseous CO_2 to form a bicarbonate. Our results indicate that adding a support or promoter or using a special technique to expose more (001)-1 surfaces in hexagonal K_2CO_3 may improve the conversion of CO_2 to the bicarbonate, which provides a theoretical direction for the experimental preparation of the K_2CO_3 sorbent to capture CO_2.

1. Introduction

With the sharp rise in the consumption and demand for fossil fuels, CO_2 (carbon dioxide) emissions will correspondingly increase unless an effective capture strategy can be put in place. It is well known that CO_2, which is a greenhouse gas, can cause global warming.[1–3] Researchers estimate that if uncontrolled greenhouse gas emissions continue, then from 1990 to 2100, the average global temperature will have increased by 1.4 °C to 5.8 °C, with a corresponding rise in sea level by 0.09 to 0.88 m, together with increased droughts, expanding deserts, heat waves, and widespread disruption to the ecosystem.[4–6] Therefore, carbon dioxide capture must be enforced.

The power plants in which coal is used as the main source for electric power produce emit flue gas accompanied by much CO_2 in most countries. Therefore, it is necessary to capture CO_2 from flue gas. Lots of techniques have been used to remove carbon dioxide from fuel gas.[7–12] The cheapest and most efficient involve sorbents, which comprise alkali and alkaline earth metals for CO_2 capture due to their high CO_2 absorption capacity at moderate working temperatures; in particular, much focus has been on potassium carbonate (K_2CO_3) as a solid sorbent for CO_2 capture.[13–18]

Potassium carbonate has a high CO_2 removal capacity and good energy efficiency, and consequently much work has been performed around it through experimental research, with different results obtained in different works. For example, Lee *et al.*[19–25] and Chen *et al.*[26–29] investigated the characteristics of pure K_2CO_3 for CO_2 capture and found that the carbonation reactivity does not originate from pure K_2CO_3 but rather originates from $K_2CO_3{\cdot}1.5H_2O$. Hirano *et al.*[30] and Hayashi *et al.*[31] supported the above results, confirming that $K_2CO_3{\cdot}1.5H_2O$ is an important intermediate species for CO_2 capture. However, Mahinpey *et al.*[32] thought that $K_2CO_3{\cdot}1.5H_2O$ could not be directly converted to $KHCO_3$. In addition, K_2CO_3 carbonation and hydration are competing reversible reactions that occur in parallel through direct reaction with the flue gas components. Theoretical calculations about the capture of CO_2 by K_2CO_3 have rarely been performed; although, Duan *et al.*[33] using first-principles density functional theory in view of the thermodynamics, identified that the $K_2CO_3/KHCO_3$ system is the most promising candidate for both pre- and post-combustion CO_2 capture. Gao *et al.*[34] studied the adsorption of CO_2 and H_2O on K_2CO_3 surface, and the result showed that H_2O is adsorbed much stronger than CO_2. However, only the CO_2 and H_2O adsorption and bicarbonate formation on the most stable (001) surface of monoclinic K_2CO_3 crystal were investigated. It is well known that K_2CO_3 has two crystal structures, *i.e.*, monoclinic and hexagonal crystal geometries. Zhao *et al.*[35] investigated the effect of the crystal structure on the CO_2 capture characteristics of dry

[a] *Key Laboratory of Coal Science and Technology of Ministry of Education and Shanxi Province, Taiyuan University of Technology, No. 79 West Yingze Street, Taiyuan 030024, Shanxi, P. R. China. E-mail: wangbaojun@tyut.edu.cn, wbj@tyut.edu.cn*

[b] *College of Chemistry and Environmental Engineering, Shanxi Datong University, No. 1 Xingyun Street, Datong, Shanxi 037009, China*

[c] *College of Chemistry and Chemical Engineering, Taiyuan University of Technology, No. 79 West Yingze Street, Taiyuan 030024, Shanxi, P. R. China*

† Electronic supplementary information (ESI) available. See DOI: 10.1039/c7cp02579c

potassium-based sorbents. Under a temperature of 338 K, the carbonation reaction was attempted with a gas composition of 10% CO_2, 10% H_2O, and N_2 balance at 500 mL min^{-1}, and they found that the carbonation reactivity of K_2CO_3 with a monoclinic crystal structure was weak, while K_2CO_3 with a hexagonal crystal structure showed excellent carbonation capacity. However, Nader Mahinpey *et al.*[36] reported that the sorbent structure with a much high reactivity was a slightly different monoclinic phase of K_2CO_3 as tested when the relative humidity of the carbonation gas was about 17% in the reactor at 323 K. In general, K_2CO_3 with a monoclinic crystal structure was obtained from dehydrated $K_2CO_3{\cdot}1.5H_2O$, while K_2CO_3 with a hexagonal crystal structure was obtained from calcined $KHCO_3$. However, in the previous experiment, the K_2CO_3 precursors were only subjected to one regeneration–carbonation cycle at 473 K, while in the latter one they were subjected to 50 regeneration–carbonation cycles at the temperatures of 423 K and 323 K. In addition, the latter experiment confirmed that, after sufficient cycling, the carbonation performances were independent of the K_2CO_3 precursors and stabilized at similar final conversions related to the carbonation conditions.

Reports on the carbonation reaction mechanism on solid K_2CO_3 from the above studies thus remain conflictive. Therefore, in order to comprehensively assess the characteristics of the K_2CO_3 capture of CO_2, we investigated different degrees of dry surfaces involved in the monoclinic and hexagonal crystals. Furthermore, we investigated the carbonation reaction on surfaces with different structures of K_2CO_3. The research aim was to clarify the mechanisms behind bicarbonate formation and the optimum structure of K_2CO_3 in CO_2 capture, as well as to achieve a more fundamental understanding of CO_2 capture by potassium carbonate at the atomistic level and to provide theoretical clues for further experimental work.

2. Computational details

2.1 Computational methods

In this study, DFT calculations were performed to evaluate the CO_2 and H_2O adsorption and carbonation reaction processes on potassium carbonate surfaces using periodic slab models. DFT has been widely used to describe the interactions between molecules and minerals.[37–39] All the calculations were performed using the Cambridge Sequential Total Energy Package (CASTEP)[40] in Materials Studio 8.0 from Accelrys, together with the General Gradient Approximation (GGA) Perdew–Wang 1991 (PW91) functional.[41] The DFT-D3 correction[42] was incorporated with the PW91 functional to handle dispersion interactions, whereby a large convergence of the plane wave expansion was obtained with an energy cut-off of 340 eV. For geometry optimization, the Brillouin zone was sampled in a $2 \times 2 \times 1$ Monkhorst–Pack set. The geometries were not optimized until the energy, force, and the max displacement had converged to 2.0×10^{-5} eV per atom, 0.05 eV $Å^{-1}$, and 2×10^{-3} Å, respectively. Spin polarization was considered throughout all the calculations.

The surface energy is defined as a function of the discrepancy between the total energies of the system before and after the deformation, which quantifies the disruption of intermolecular bonds formed during creation of a surface.[43] The specific surface energy was calculated by the following formula:

$$E_{\text{surface}} = [E_{\text{slab}} - N \times E_{\text{bulk}}]/2A$$

where E_{slab} refers to the total energy of the slab, E_{bulk} is the energy of atoms each layers, N is the number of layers, and A is the surface area. A vacuum region of 15 Å was added above the surface to ensure negligible interaction between periodic images normal to the surface. In calculating the surface energy, the middle layer was frozen at bulk K_2CO_3 coordinates to accelerate the surface energy convergence with respect to the slab thickness.

The adsorption energy is defined as:

$$E_{\text{ads}} = E_{(\text{surface+adsorbate})} - (E_{\text{surface}} + E_{\text{adsorbate}})$$

where $E_{(\text{surface+adsorbate})}$ is the total energy of the surface with the adsorbate, $E_{\text{adsorbate}}$ is the energy of the free adsorbate, and E_{surface} is the total energy of the surface.

The interaction energy between the adsorbates is defined as:

$$E_{\text{inter}} = E_{(CO_2+H_2O+\text{surface})} + E_{\text{surface}} - E_{(CO_2+\text{surface})} - E_{(H_2O+\text{surface})}$$

where $E_{(CO_2+H_2O+\text{surface})}$ is the total energy of H_2O and CO_2 co-adsorbed on the K_2CO_3 surface, $E_{(CO_2+\text{surface})}$ is the energy of CO_2 adsorbed on the K_2CO_3 surface, and $E_{(H_2O+\text{surface})}$ is the energy of H_2O adsorbed on the K_2CO_3 surface.

In addition, the activation energy E_a and reaction energy ΔE were calculated according to the following formulas:

$$E_a = E_{TS} - E_R$$

$$\Delta E = E_P - E_R$$

where E_R, E_{TS}, and E_P are the energies of the reactants, transition states, and products, respectively, in the first equation, and E_a is the activation energy of the reaction, while ΔE is the reaction energy in the latter equation.

2.2 Computational model

2.2.1 Model of the bulk. The lattice parameters of bulk K_2CO_3 were obtained from the Inorganic Crystal Structure Database (ICSD). Bulk K_2CO_3 has two crystal systems: monoclinic and hexagonal. K_2CO_3 with a monoclinic crystal structure belongs to the $P121/c1$ space group with four formula units in the primitive cell. However, K_2CO_3 with a hexagonal crystal structure belongs to the $P63/m$ space group with two formula units in the primitive cell, which is a monoclinic high-temperature modification of potassium carbonation.

2.2.2 Model of surface. Based on the crystalline structure, models of low-index surfaces of potassium carbonate were constructed. The methods to cut the crystal and obtain various surfaces are detailed in the ESI,† illustrated in Fig. 1S. Stoichiometric surfaces were obtained through cutting the crystal. In calculating the surface energies, different layers were taken into account when a surface was created, and all the atoms were relaxed.

In investigating the carbonate reaction, a 2 × 1 periodic slab model was used to model the surface, with the slab containing three molecular layers, with the bottom layer kept frozen at bulk optimized positions and the upper two layers allowed to relax. The vacuum thickness (size of unit cell perpendicular to the slab–slab thickness) was set at 15 Å, which is large enough to avoid unnecessary potential surface–surface interactions. Optimization of an isolated gas molecule was performed in a large cubic box of 10 Å × 10 Å × 10 Å.

3. Results and discussion

3.1 Bulk K_2CO_3

The optimized crystal structures of bulk K_2CO_3 with monoclinic and hexagonal phases are shown in Fig. 1(a) and (b), respectively. The DFT calculated structural parameters are listed in Tables 1 and 2, along with the experimental structural data.[44] In comparison with the experimental values, the relative deviations between our calculated structure parameters and the experimental values were within 5%, indicating that, under the above parameter settings, the DFT calculations are reliable.

3.2 Surface energies

The K_2CO_3 carbonation reaction can be described by the unreacted-core model, where CO_2 adsorption and reactions occur on a heterogeneous surface. Hence, the crystal surface that is to be considered as the reaction surface should be determined primarily. Fig. 2 displays the top views of the surfaces for the (001), (010), (011), (100), (101), (110), and (111) surfaces of monoclinic crystal K_2CO_3, and the (001), (010), (011), (110), and (111) surfaces of hexagonal crystal K_2CO_3, respectively. The side views of those surfaces are shown in Fig. 2S in the ESI.†

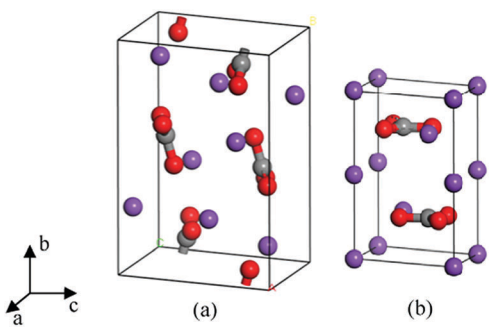

Fig. 1 Optimized crystal structures of bulk K_2CO_3: (a) monoclinic crystal, (b) hexagonal crystal. Red, O; purple, K; and black, C.

Table 1 Optimized structural parameters and experimental values for the monoclinic K_2CO_3

Structural parameters	a/Å	b/Å	c/Å	$\alpha = \gamma$/°	β/°	O1–C/Å	O2–C/Å	O3–C/Å
EXP.[a]	5.64	9.83	6.83	90.0	98.7	1.27	1.28	1.29
GGA/PW91	5.66	9.80	6.71	90.0	99.0	1.30	1.31	1.31
Relative deviation (%)	0.35	0.31	1.76	0	0.31	2.36	2.34	1.55

[a] Experimental values from ref. 44.

Table 2 Optimized structural parameters and experimental values for hexagonal K_2CO_3

Structural parameters	$a = b$/Å	c/Å	$\alpha = \beta$/°	γ/°	O1–C/Å	O2–C/Å	O3–C/Å
EXP.[a]	5.66	7.10	90.0	120.0	1.28	1.28	1.28
GGA/PW91	5.66	7.34	90.0	120.0	1.31	1.31	1.31
Relative deviation (%)	0.00	3.38	0.00	0.00	2.34	2.34	2.34

[a] Experimental values from ICSD-52535.

It is worth noting that the (001) surface of the hexagonal crystal K_2CO_3 can be terminated in two different ways, either by a layer of potassium atoms (marked (001)-1) or by carbonate groups (marked (001)-2), as shown in Fig. 3S in the ESI,† which are not identical polar surfaces. To determine the stability of various surfaces, we evaluated the surface energies of the various low-index terminations. Notably, the (100) and (101) surfaces of hexagonal K_2CO_3 were similar to the (010) and (011) surfaces, respectively. The specific surface energy (E_{surf}) was also calculated, and the resulting values of the surface energies and their averages for all the surfaces of K_2CO_3 are listed in Table 1S (ESI†). In particular, the (001)-1 and (001)-2 surfaces in hexagonal K_2CO_3 have the same surface energies; therefore, the surface energies for the two surfaces are not listed separately.

According to the average surface energy, the stability orders of the surfaces in monoclinic and hexagonal K_2CO_3 are (001) > (011) > (100) > (111) > (101) > (110) > (010) and (111) > (011) > (110) > (001) > (010), respectively. Certainly, the (001) surface is more stable and more easily obtained when monoclinic crystal K_2CO_3 is cleaved or in nature, which is consistent with the calculated results by Gao *et al.*[34]

3.3 CO_2 and H_2O adsorption

3.3.1 Monoclinic K_2CO_3 surface. Bicarbonate formation is based on the adsorption of CO_2 and H_2O. Therefore, the isolated adsorptions of CO_2 and H_2O on the above-mentioned surfaces were investigated first. Different CO_2 and H_2O adsorption configurations on the monoclinic K_2CO_3 surfaces were explored by geometrical optimization and the stable adsorption configurations were found and are shown in Fig. 3. The adsorption energies (E_{ads}) and structural parameters as well as Mulliken charges are given in Table 3.

For the CO_2 adsorption on the monoclinic crystal surfaces, the most stable configurations on the above-mentioned surfaces are shown in Fig. 3(a). The C–O bond lengths in the adsorbed CO_2 on the different surfaces of monoclinic K_2CO_3 were slightly longer or shorter than that in isolated gaseous state, while the bond angles of the adsorbate were reduced on all the surfaces compared to those in the gas phase. Analyzing the Mulliken charge, it was found that there are electrons transferred from the surface to the C–O anti-bonding orbitals, which makes the C–O bond change. The calculated adsorption energies were −0.43 to −0.57 eV on the surfaces. Although the value of adsorption energy for CO_2 on the (001) surface was the largest, we still considered that it was physisorbed on the surface according to the geometric parameters. Gao *et al.*[34] obtained an adsorption

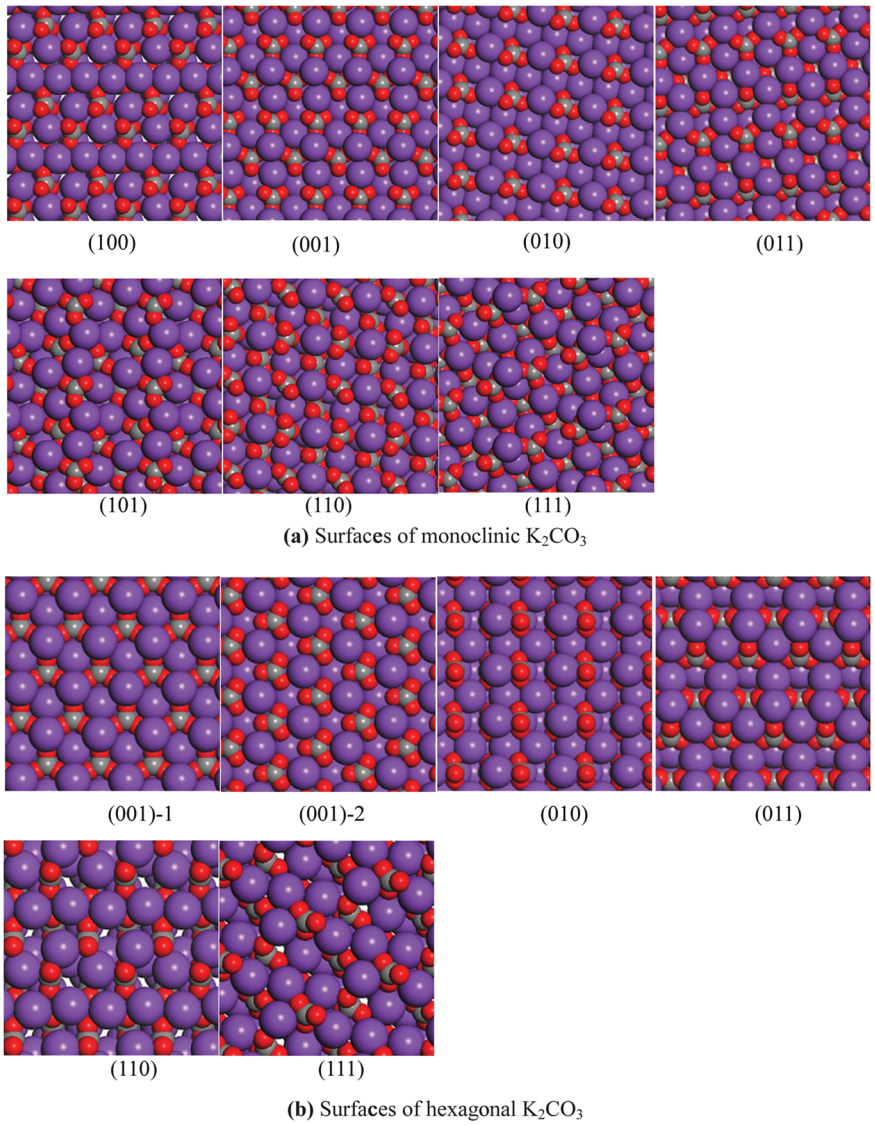

Fig. 2 Top views of the surfaces of K_2CO_3. Red, O; purple, K; and black, C.

energy of CO_2 for the most stable configuration on the (001) surface as −0.35 eV, almost consistent with our result (−0.39 eV) without dispersion correction.

For the H_2O adsorption on the monoclinic crystal surfaces, the most stable configurations on the different surfaces are shown in Fig. 3(b). The H–O bond lengths in the adsorbed H_2O were slightly longer than that the optimal value of 0.977 Å in the gas phase. The calculated adsorption energy on the surfaces were from −0.88 to −1.31 eV. The values of Mulliken charge about H_2O indicated that electrons transfer from the surface to the H–O anti-bonding orbital, which makes the H–O bond stretch.

Obviously, the adsorption of H_2O molecules is clearly substantially stronger to this surface than that of CO_2. This implies that when H_2O is strongly adsorbed first on the surface, CO_2 molecules cannot displace the adsorbed H_2O molecules, which is in agreement with the experimental observations of Zhao *et al.*[45] Therefore, H_2O adsorption will first occur on K_2CO_3 with the monoclinic crystal structure, then CO_2 gas reacts with the adsorption molecules of H_2O in the carbonation reaction.

3.3.2 Hexagonal K_2CO_3 surface. Same as on monoclinic K_2CO_3 surfaces, the molecular adsorption of CO_2 and H_2O precedes bicarbonate formation. Different CO_2 and H_2O adsorption configurations on the hexagonal K_2CO_3 surface were explored by geometry optimization and the most stable adsorption configurations were found and are shown in Fig. 4. The adsorption energies, Mulliken charges, and structural parameters are given in Table 4. It was found that the molecular geometries of the adsorbed CO_2 and H_2O were also significantly different from the free CO_2 and H_2O molecules, respectively, and even different from the adsorption on the monoclinic K_2CO_3 surface.

As shown in Fig. 4(a), the C–O bond lengths in the adsorbed CO_2 on different surfaces were slightly longer or shorter than the gas phase optimal value of 1.184 Å, while the bond angle in the adsorbate is decreased compared to the optimal value of

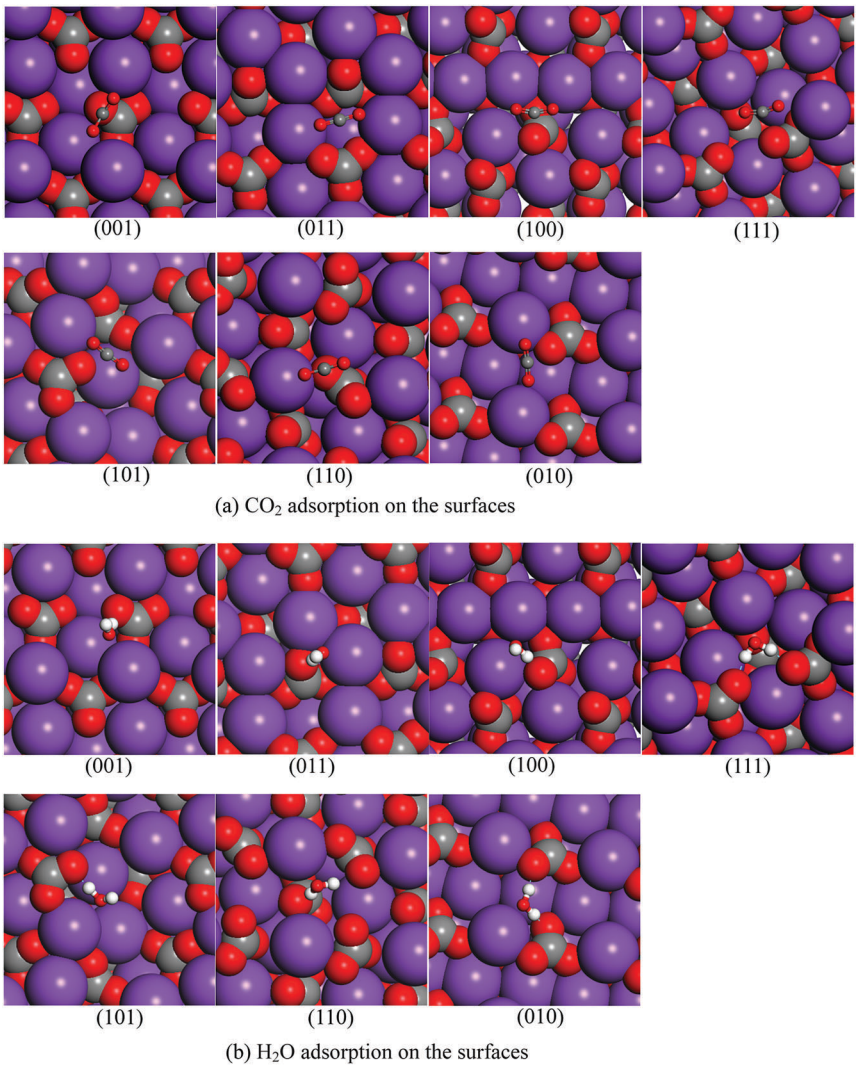

Fig. 3 Top views of the optimized structures of CO_2 and H_2O adsorption on the (001), (011), (100), (111), (101), (110), and (010) surfaces of monoclinic K_2CO_3, respectively. Red, O; purple, K; and black, C.

180.0° in the gas phase, because of the partial electron transfer from the surface O atoms to the C–O anti-bonding orbitals. The calculated adsorption energies on those surfaces were −0.32 to −0.83 eV. Physisorption on the (111), (011), (110), (001)-2, and (010) surfaces could be clearly seen. Interesting, for (001)-1, the bond angle for adsorbed CO_2 showed a significant change, while the adsorption energy was as high as −0.83 eV, indicating chemisorption on the (001)-1 surface.

For the H_2O adsorption on the hexagonal crystal surface, the geometries were optimized and the most stable configurations on different surfaces are shown in Fig. 4(b). The H–O bond lengths in the adsorbed H_2O were longer than the optimal value of 0.977 Å in the gas phase, because partial electrons transfer from the surface O atoms to the H–O anti-bonding orbitals. The calculated adsorption energies on different surfaces were −0.81 to −1.48 eV. It could clearly be seen that all the configurations had a chemisorbed structure involving a strong hydrogen bond to a surface O atom and additional dipole-K interactions. In particular, the most stable adsorption of H_2O was on the (010) surface. Certainly, H_2O was chemisorbed on all the surfaces of monoclinic and hexagonal K_2CO_3.

In conclusion, the adsorption of the H_2O molecule is clearly substantially stronger to this K_2CO_3 surface than the adsorption of CO_2. Interestingly, the adsorption energy of CO_2 on (001)-1 surface was almost equal to the energy of adsorption H_2O on the (001)-1 surfaces, indicating that CO_2 and H_2O competitively chemisorb on the (001)-1 surface of hexagonal K_2CO_3.

3.3.3 CO_2 and H_2O co-adsorption. Because the adsorption of the polar H_2O molecule is clearly substantially stronger to this K_2CO_3 surface than the adsorption of CO_2, except on the (001)-1 surface of the hexagonal crystal, in the study of the co-adsorption of CO_2 and H_2O, CO_2 was adsorbed on the stable surface with H_2O pre-adsorption. Then, we evaluated various co-adsorption configurations for H_2O and CO_2 on the K_2CO_3 surfaces. The optimized co-adsorption structures of CO_2 and H_2O adsorbed on the monoclinic K_2CO_3 surfaces as well as on the hexagonal K_2CO_3 surfaces are shown in Fig. 5. The co-adsorption structural parameters and co-adsorption energies are given in Tables 2S and 3S (ESI†).

Table 3 Adsorption structural parameters, adsorption energies, and Mulliken charges for CO_2 and H_2O adsorption on the monoclinic K_2CO_3(001), (011), (100), (111), (101), (110), and (010) surfaces, respectively

Structure	d_{H-Os}/d_{C-Os} (Å)	d_{O-K}/d_{O-K} (Å)	Bond distance within adsorbate (Å)	Bond angle of adsorbate (deg)	E_{ads} (eV) Not corrected	E_{ads} (eV) Dispersion corrected	Mulliken charge (e)
CO_2			1.184	180.0			
(001)	2.354	3.028/3.582	1.184/1.192	165.6	−0.39	−0.57	−0.15
(011)	3.199	2.948/3.133	1.181/1.183	177.9	−0.24	−0.44	−0.10
(100)	2.079	2.937/3.140	1.203/1.204	154.7	−0.38	−0.56	−0.32
(111)	2.315	2.767/3.350	1.190/1.193	160.7	−0.38	−0.56	−0.22
(101)	2.603	3.336/3.396	1.185/1.186	172.9	−0.38	−0.55	−0.11
(110)	2.529	2.792/4.389	1.180/1.187	173.6	−0.26	−0.43	−0.11
(010)	2.516	2.983/2.834	1.181/1.228	174.6	−0.37	−0.56	−0.14
H_2O			0.977	104.8			
(001)	1.522	2.799	0.974/1.039	105.6	−0.96	−1.15	0.24
(011)	1.573	2.755	0.975/1.020	108.6	−0.71	−0.88	−0.05
(100)	1.559	2.775	0.976/1.040	105.5	−0.93	−1.12	−0.19
(111)	1.764/1.973	3.063	0.991/1.003	101.7	−0.94	−1.19	−0.16
(101)	1.675	2.653	0.973/1.040	105.5	−1.03	−1.24	−0.21
(110)	1.774/2.100	2.880	0.986/0.994	105.5	−0.65	−0.89	−0.15
(010)	1.709/2.021	2.761	0.991/1.007	103.8	−1.08	−1.31	−0.23

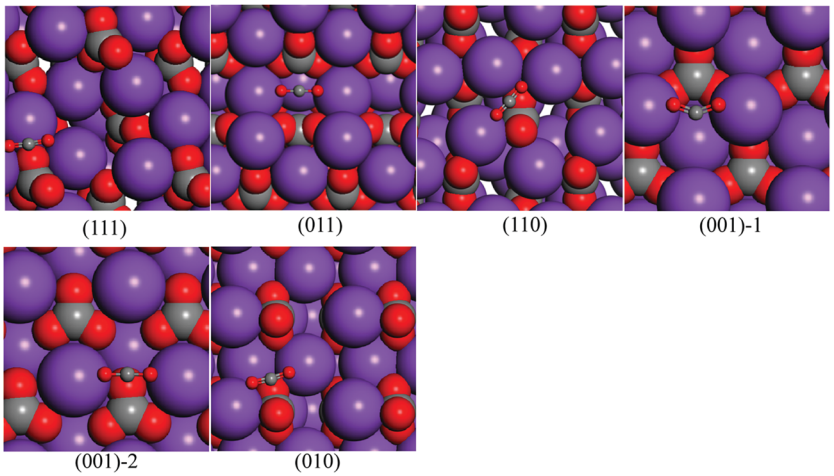

(a) CO_2 adsorption on the surfaces

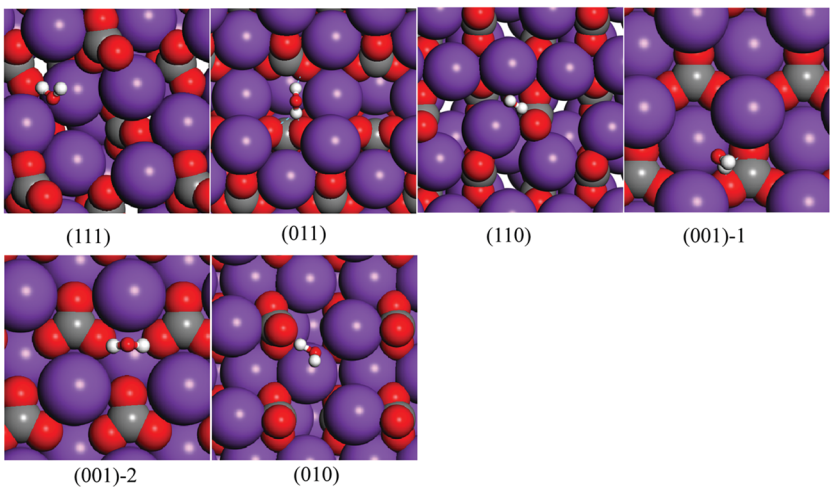

(b) H_2O adsorption on the surfaces

Fig. 4 Top views of the optimized structures of CO_2 and H_2O adsorption on the (111), (011), (110), (001)-1, (001)-2, and (010) surfaces of hexagonal K_2CO_3, respectively. Red, O; purple, K; and black, C.

Table 4 Adsorption structures and adsorption energies as well as Mulliken charge for CO_2 and H_2O adsorption on the hexagonal K_2CO_3(111), (011), (110), (001)-1, (001)-2, and (010) surfaces, respectively

Structure	d_{H-Os}/d_{C-Os} (Å)	d_{O-K}/d_{O-K} (Å)	Bond distance within adsorbate (Å)	Bond angle of adsorbate (deg)	E_{ads} (eV) Not corrected	E_{ads} (eV) Dispersion corrected	Mulliken charge (e)
CO_2			1.184	180.0			
(111)	2.606	3.003/3.625	1.188/1.178	174.1	−0.20	−0.34	−0.14
(011)	3.368	3.282/3.322	1.181/1.184	177.0	−0.33	−0.53	−0.11
(110)	2.676	2.858/3.280	1.179/1.181	174.4	−0.19	−0.35	−0.14
(001)-1	—	2.646/2.667	1.246/1.249	139.5	−0.72	−0.83	−0.68
(001)-2	3.234	3.152/3.128	1.182/1.180	177.8	−0.16	−0.32	−0.08
(010)	2.431	2.920/3.513	1.190/1.176	171.0	−0.36	−0.52	−0.13
H_2O			0.977	104.8			
(111)	1.645	2.683	1.019/0.976	108.3	−0.76	−0.97	−0.19
(011)	2.025/2.008	3.130	0.943/0.987	104.4	−0.74	−1.00	−0.16
(110)	1.877	2.804	0.978/1.000	107.3	−0.76	−0.91	−0.13
(001)-1	1.814	2.914	0.978/1.006	106.5	−0.67	−0.86	−0.17
(001)-2	1.966/1.893	3.101	0.991/0.988	100.9	−0.58	−0.81	−0.17
(010)	1.489	2.829	1.058/0.977	103.0	−1.30	−1.48	−0.18

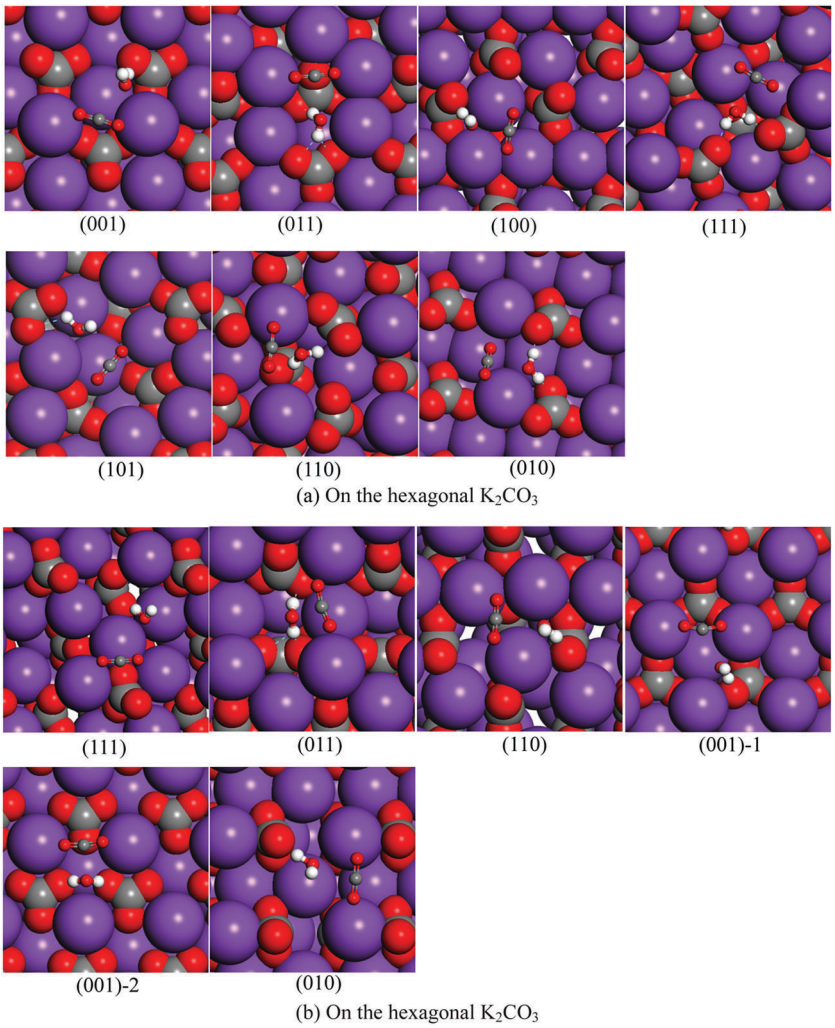

Fig. 5 Top views of the optimized co-adsorption structures of CO_2 and H_2O on K_2CO_3 surfaces. Red, O; purple, K; black, C and white, H.

The data suggests that in the case of co-adsorption configurations, CO_2 is disadvantage of adsorption on the monoclinic (010) surface and hexagonal (001)-1 surface, However, CO_2 is advantage of adsorption on the hexagonal (011) and (001)-2 surfaces.

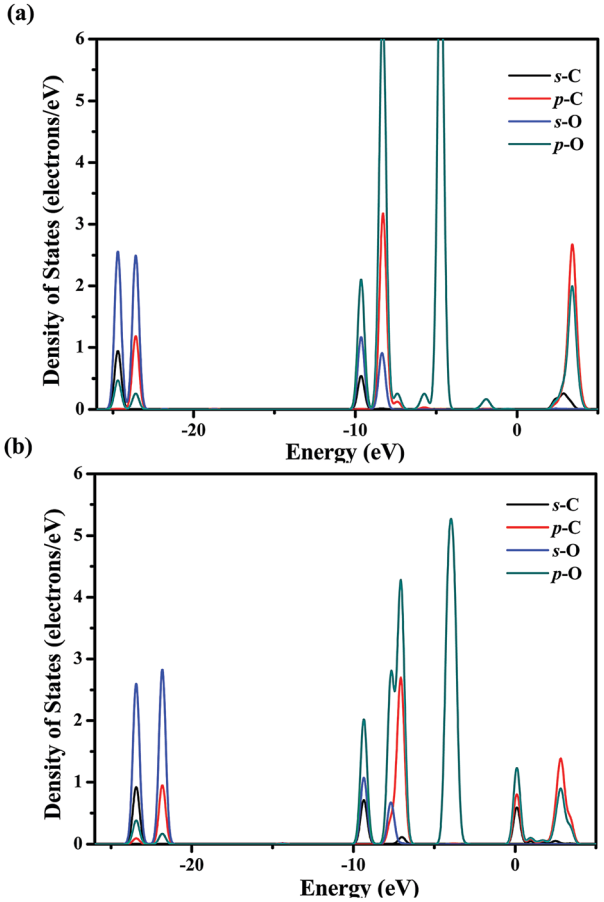

Fig. 6 PDOS plots for adsorbed CO_2: (a) CO_2 adsorption on the (001) surface of monoclinic K_2CO_3; (b) CO_2 adsorption on the (001)-1 surface of hexagonal K_2CO_3.

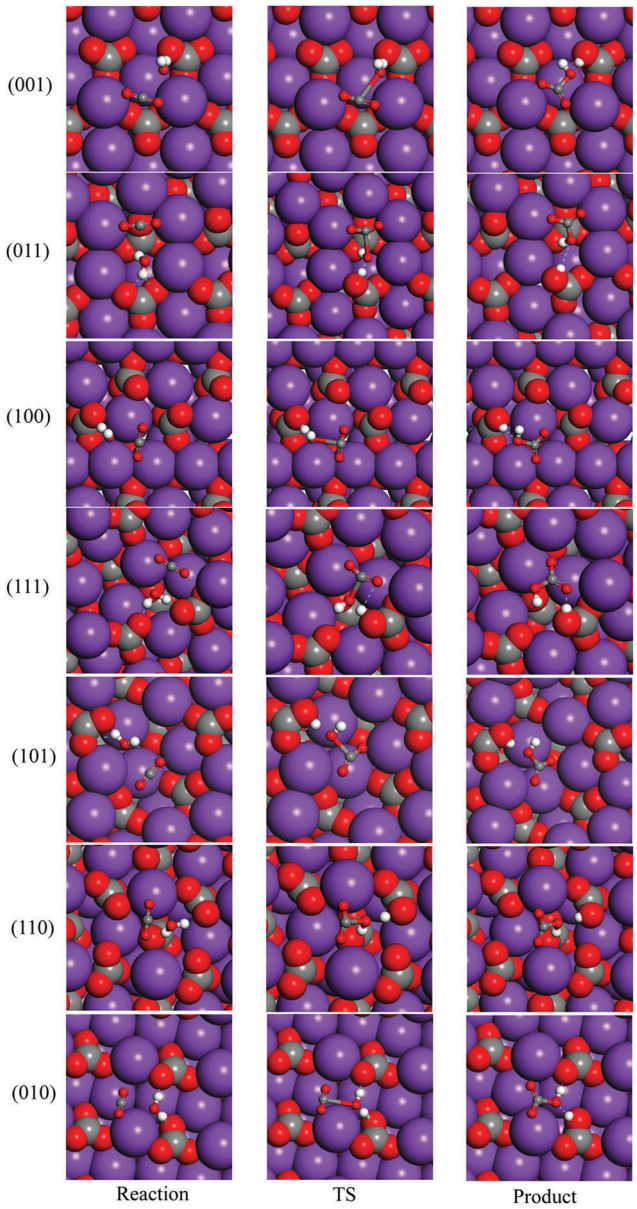

Fig. 7 Optimized geometries of the reactant, transition state (TS) and product for bicarbonate formation on the surface of monoclinic K_2CO_3: (001), (011), (100), (111), (101), (110), and (010). Red, O; purple, K; black, C; and white, H.

3.3.4 PDOS analysis. In order to gain insights into the electronic structure to further understand and confirm our calculated results, the project density of states (PDOSs) of CO_2 adsorption on the (001) surface of monoclinic K_2CO_3 and on the (001)-1 of hexagonal K_2CO_3 were analyzed, and the results are shown in Fig. 6. This figure shows that the s- and p-orbitals of CO_2 adsorbed on the (001) surface of monoclinic K_2CO_3 were in the range of −25.4 to −23.9 eV below the Fermi level. However, when CO_2 was adsorbed on the (001)-1 surface of hexagonal K_2CO_3, the s- and p-orbitals upshift to −24.2 to −22.7 eV, closer to the Fermi level than the former, indicating that CO_2 is activated on the (001)-1 surface of hexagonal K_2CO_3. On the other hand, the total areas of the s- and p- orbitals from C and O were increased when CO_2 was adsorbed on the (001)-1 surface of hexagonal K_2CO_3 compared to those on the (001) surface of monoclinic K_2CO_3, indicating that it obtained more electrons on the hexagonal K_2CO_3(001) surface that that on monoclinic K_2CO_3(001)-1. Clearly, the PDOS analysis results are consistent with our calculated results for the Hirshfeld charge and adsorption energy.

3.4 Mechanism of the carbonation reaction

Although CO_2 molecules can adsorb on the K_2CO_3 surface, such adsorption of CO_2 and H_2O on the surface does still not explain the carbonate process. Hence, in order to gain an insight into the CO_2-capture characteristics by K_2CO_3, we also investigated the bicarbonate formation based on the most stable adsorption configurations for H_2O and CO_2 on different surfaces of K_2CO_3.

3.4.1 One-step mechanism. For the bicarbonate formation, first we considered a path in which the OH group breaks from H_2O and attacks the C atom of CO_2, based on the most stable co-adsorption configurations for H_2O and CO_2. The optimized geometries of the reactants, transition state (TS), and the product for the bicarbonate formation reaction on each surface are shown in Fig. 7 and 8, while the structural parameters and activation energy as well as the reaction heat are listed in Table 5.

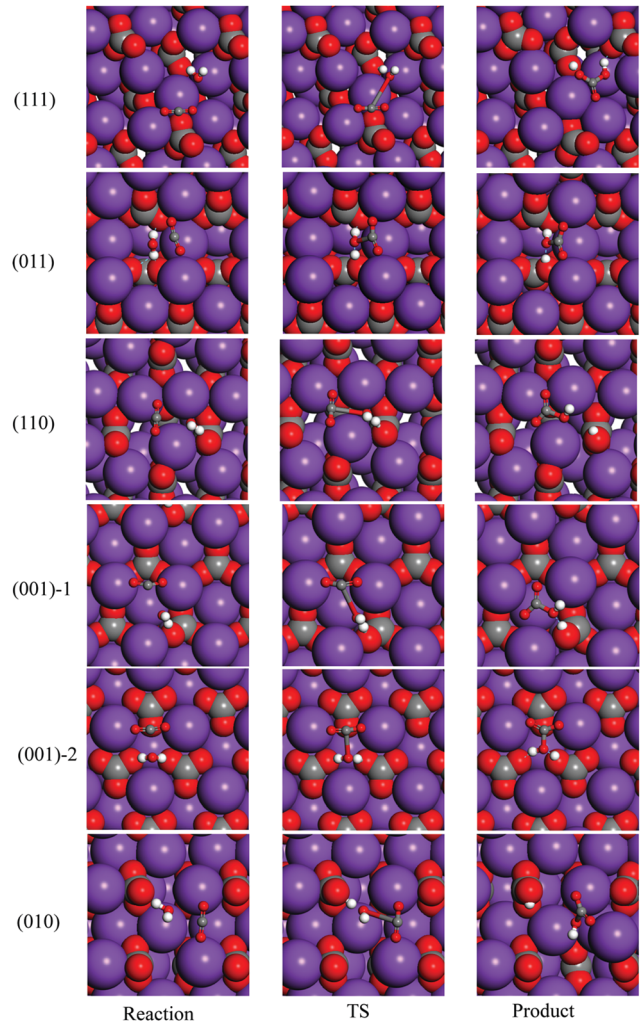

Fig. 8 Optimized geometries of the reactant, transition state (TS) and product using DFT for bicarbonate formation on the surface of hexagonal K_2CO_3: (111); (011); (110); (001)-1; (001)-2, and (010) surfaces, respectively. Red, O; purple, K; black, C; and white, H.

In all cases, the H–O bond in the adsorbed H_2O was broken, then prolonged to 1.025–1.968 Å, while a bond between the C atom in CO_2 and O atom in H_2O is formed, and the distance is shortened to 1.461–3.080 Å, and the O–C–O angle of adsorbed CO_2 becomes smaller, about 135°. On those surfaces of monoclinic K_2CO_3, the activation energies were 0.20 to 0.50 eV, which was almost in agree with the results obtained by Gao *et al.* (0.30 eV)[34] and Zhao *et al.* (0.35 eV).[46] The reaction energies were negative, indicating that it is an exothermic reaction. On the (010) and (111) surfaces of hexagonal K_2CO_3, the activation energies were 0.73 and 0.65 eV, thus higher than those on the monoclinic K_2CO_3 surfaces. On the other surfaces of hexagonal K_2CO_3, the activation energies were relatively lower; however, the reaction energies were positive. In order to judge whether the reaction can occur on monoclinic and hexagonal K_2CO_3, we plotted the potential energy for the carbonation reaction, as shown in Fig. 4S (ESI†). Certainly, the overall reaction was exothermic on all the surfaces, and the reaction barriers were relative low. Therefore, one can conclude that bicarbonate formation easily occurs on the monoclinic and hexagonal K_2CO_3 surfaces through a "one-step" process, *i.e.*, an OH group breaks from H_2O and attacks the C atom of CO_2 at the same time.

3.4.2 Two-step mechanism. Another path was also considered herein, in which water dissociation preceded bicarbonate formation (denoted step 1), then the OH group from the water dissociation reacts with the gas molecule of CO_2 (denoted step 2). We only obtained the structure of the product from H_2O dissociation on the monoclinic (001) and (011) surfaces and on the hexagonal (010) surface. On the other surfaces, the products of H_2O dissociation were not stable, and they easily returned to the reactant after optimization. The optimized geometries of the reactants, the transition state (TS), and the product for the water dissociation reaction on each surface are shown in Fig. 9. The structural parameters, activation energies (E_a), and reaction energies (ΔE) on the monoclinic (001) and (011) surfaces and on the hexagonal (010) surface are shown in Table 6. Certainly, the water dissociation reaction on the monoclinic (001) and

Table 5 Transition state structural parameters (bond length, Å; bond angle, °), activation energies (E_a, eV), and reaction energies (ΔE, eV) for CO_2 and H_2O reaction on the monoclinic and hexagonal K_2CO_3 for each surface, respectively

Structure	Surface	d_{C-O1}[a]	d_{C-O2}[a]	d_{H1-O}[b]	d_{H2-O}[c]	d_{C-O}[d]	O–C–O[e]	E_a	ΔE
Monoclinic	(001)	1.203	1.210	0.979	1.353	2.228	157.1	0.24	−0.44
	(011)	1.180	1.196	1.008	1.337	2.335	154.5	0.50	−0.32
	(100)	1.176	1.188	0.977	1.054	2.401	173.6	0.19	−0.20
	(111)	1.188	1.193	0.979	1.103	2.076	151.1	0.33	−0.86
	(101)	1.211	1.223	0.976	1.409	2.014	147.9	0.38	−0.46
	(110)	1.220	1.224	0.998	1.398	1.904	148.5	0.20	−0.09
	(010)	1.248	1.263	1.020	1.740	1.461	130.9	0.27	−0.18
Hexagonal	(111)	1.207	1.235	0.991	1.968	2.505	149.5	0.65	−0.48
	(011)	1.214	1.215	0.985	1.655	1.955	150.1	0.49	0.19
	(110)	1.178	1.184	0.978	1.025	2.766	178.1	0.64	0.30
	(001)-1	1.245	1.253	0.978	1.012	3.080	137.0	0.60	0.25
	(001)-2	1.191	1.225	0.992	1.129	1.906	146.2	0.47	0.24
	(010)	1.173	1.181	0.978	1.060	3.026	177.7	0.73	−0.83

[a] d_{C-O1} and d_{C-O2} are the bond distances (Å) between the C atom and the O atom in adsorbed CO_2. [b] d_{H1-O} is the distances (Å) between the H atom and O atom of the OH group breaking from H_2O. [c] d_{H2-O} H atom breaks from H_2O and the O atom of the OH group breaks from H_2O. [d] d_{C-O} is the distance (Å) between the C atom of CO_2 and the O atom of the OH group breaking from H_2O. [e] O–C–O is the bond angle (deg) in adsorbed CO_2.

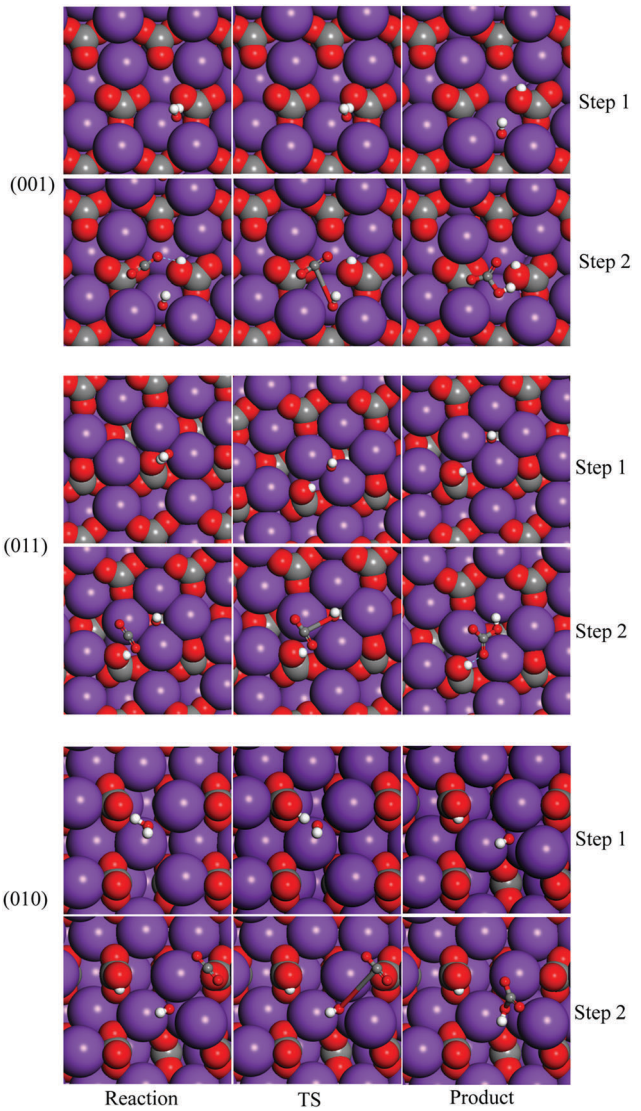

Fig. 9 Optimized geometries of the reactant, transition state (TS), and product using DFT for the water dissociation reaction as well as the CO_2 reaction with an OH break from H_2O: (001) and (011) surfaces of the monoclinic crystal K_2CO_3 and (010) surface of the hexagonal crystal K_2CO_3, respectively. Step 1: the water dissociation; step 2: the OH group from water dissociation reacts with the gas molecule of CO_2; Red, O; purple, K; black, C; and white, H.

(011) surfaces was endothermic with a much high activation energy of 1.62 and 1.38 eV. However, on the hexagonal (010) surface, the water dissociation was exothermic and had a low activation energy of 0.57 eV. Then, OH from the H_2O dissociation reacted with CO_2 with a very low activation energy of 0.26 eV and reaction energy of 0.09 eV. Although the second step was slightly endothermic, the reaction could proceed because the first step sends out lots of heat. Similarly, we also plotted the potential energy (shown in Fig. 5S, ESI†) to confirm whether the carbonation reaction easily took place. Obviously, on the (001) and (011) surfaces for monoclinic K_2CO_3, the reactions were relatively difficult to occur because of the relatively higher reaction barriers compared to that on the (010) surface for hexagonal K_2CO_3. Based on the above results, one can conclude that the carbonation reaction is possible on the hexagonal (010) surface through a "two-step" process, *i.e.*, water dissociates first, then the OH group from the water dissociation reacts with the gaseous CO_2, which is similar to in the TiO_2-catalyzed reaction of CO_2 in the presence of H_2O.[47] Gao *et al.*[34] found that this mechanism is not favorable on the monoclinic K_2CO_3(001) surface, which is consistent with our results. However, they did not investigate the carbonation reaction on hexagonal K_2CO_3; whereas, importantly, our results confirmed that the mechanism is possible on hexagonal K_2CO_3.

Our results confirmed that the carbonation reaction can directly proceed either *via* an OH group breaking off from H_2O and attacking the C atom of CO_2 at the same time on monoclinic and hexagonal K_2CO_3 or *via* water dissociating first, and then the OH group from the water dissociation reacts with the gaseous CO_2 on hexagonal K_2CO_3. Although the carbonation reaction may proceed at the electronic level, the coverage of CO_2 is exceedingly small except on the (001)-1 surface of hexagonal K_2CO_3 because of the weak adsorption of CO_2 on monoclinic K_2CO_3, while the strong adsorption on hexagonal K_2CO_3(001)-1 surface is based on the hypothesis of competitive Langmuir adsorption and excludes possible other possible adsorbates, therefore the carbonation reactivity was weak on monoclinic K_2CO_3, while it is excellent on hexagonal K_2CO_3. This conclusion is consistent with the experiment results.[35] However, the (001)-1 surface from hexagonal K_2CO_3 has high surface energy, indicating it is not stable, and has a short lifetime, and is even absent in the K_2CO_3 sorbent; therefore, in preparation, a support, promoter, or a special technique is needed to make the (001)-1 surface stable, and at the same time, to modify the structure of other surfaces to strength the adsorption of CO_2, to further improve the conversion to the bicarbonate.

Table 6 Transition state structural parameters (bond length, Å; bond angle, °), activation energies (E_a, eV), and reaction energies (ΔE, eV) for CO_2 and H_2O reaction on the monoclinic and hexagonal K_2CO_3 for each surface, respectively

Structure	Surface	d_{H1-O}[a]	d_{H2-O}[b]	d_{C-O1}[c]	d_{C-O2}[c]	d_{C-O}[d]	O–C–O[e]	E_a-S1	ΔE-S1	E_a-S2	ΔE-S2
Monoclinic	(001)	3.862	0.987	1.178	1.180	3.302	175.8	1.56	1.02	0.35	−0.43
	(011)	2.592	0.993	1.179	1.185	2.928	173.6	1.38	1.04	0.11	−1.01
Hexagonal	(010)	1.881	0.984	1.179	1.179	4.847	176.9	0.57	−0.99	0.26	0.09

[a] d_{H1-O} is the distances (Å) between the H atom and the O atom of the OH group breaking from H_2O. [b] d_{H2-O} H atom breaks from H_2O and the O atom of the OH group breaks from H_2O. [c] d_{C-O1} and d_{C-O2} are the bond distances (Å) between the C atom and the O atom in the adsorbed CO_2. [d] d_{C-O} is the distance (Å) between the C atom of CO_2 and the O atom of the OH group breaking from H_2O. [e] O–C–O is the bond angle (deg) in adsorbed CO_2.

4. Conclusion

This investigation highlighted the adsorption characteristics of CO_2 and H_2O as well as bicarbonate formation on all low-index surfaces of both monoclinic crystal and hexagonal crystal K_2CO_3 using density functional theory. The adsorption structures, adsorption energies, and barriers of bicarbonate formation for CO_2 and H_2O adsorbed on the K_2CO_3 surfaces are reported. The results showed that the adsorption of CO_2 on all surfaces was weaker than that of H_2O except on the hexagonal system (001)-1 surface, where the adsorption energy of CO_2 was equal to the energy of adsorption of H_2O. The carbonate reaction had a low activation energy on the two kinds of crystal surfaces of K_2CO_3 through one-step and two-step mechanisms. On the monoclinic and hexagonal K_2CO_3, the H_2O molecules were more likely to be adsorbed first, then the CO_2 gas reaction proceeded with the adsorption of H_2O. However, on the (010) surface with the hexagonal K_2CO_3 crystal structure, the carbonation reaction may also occur *via* water dissociating first, then the OH group from the water dissociation reacts with the gas molecule of CO_2.

The strong adsorption of CO_2 on the (001)-1 surface of hexagonal K_2CO_3 suggests that in the preparation of the K_2CO_3 sorbent, more (001)-1 surfaces from hexagonal K_2CO_3 can be exposed through the introduction of a support, promoter, or other special technique to improve the conversion to the bicarbonate. Our results provide reference both for understanding the carbonation reaction and for the preparation of better K_2CO_3 adsorbents for CO_2 capture.

Conflicts of interest

There are no conflicts to declare.

Acknowledgements

The work was supported financially by the National Natural Science Foundation of China (No. 21506120, 21276171 and 21576178) and Doctoral Scientific Research Foundation of Datong University of Shanxi (No. 2012-B-07).

References

1 M. R. Allen, D. J. Frame, C. Huntingford, C. D. Jones, J. A. Lowe, M. Meinshausen and N. Meinshausen, Warming caused by cumulative carbon emissions towards the trillionth tonne, *Nature*, 2009, **458**, 1163–1166, DOI: 10.1038/nature08019.

2 M. Meinshausen, N. Meinshausen, W. Hare, S. C. Raper, K. Frieler, R. Knutti, D. J. Frame and M. R. Allen, Greenhouse-gas emission targets for limiting global warming to 2 °C, *Nature*, 2009, **458**, 1158–1162, DOI: 10.1038/nature08017.

3 M. Allen, D. Frame, K. Frieler, W. Hare, C. Huntingford and C. Jones, The exit strategy, *Nat. Reports Climate Change*, 2009, **3**, 56–58, DOI: 10.1038/climate.2009.38.

4 P. Freund and W. G. Ormerod, Progress toward storage of carbon dioxide, *Energy Convers. Manage.*, 1997, **38**(supplement), S199–S204, DOI: 10.1016/S0196-8904(96)00269-5.

5 S. M. Klara and R. D. Srivastava, U. S. DOE integrated collaborative technology development program for CO_2 separation and capture, *Environ. Prog. Sustainable Energy*, 2002, **21**, 247–253, DOI: 10.1002/ep.670210414.

6 H. L. Lee, An emissions data base for integrated assessment of climate change policy using GTAP, *GTAP Technical Paper*, 2002.

7 B. Wang, H. Jin and D. Zheng, Recovery of CO_2 with MEA and K_2CO_3 absorption in the IGCC system, *Int. J. Engine Res.*, 2004, **28**, 521–535, DOI: 10.1002/er.982.

8 M. G. Plaza, C. Pevida and A. Arenillas, CO_2 capture by adsorption with nitrogen enriched carbons, *Fuel*, 2007, **86**, 2204–2212, DOI: 10.1016/j.fuel.2007.06.001.

9 A. Meisen and X. Shuai, Research and development issues in CO_2 capture, *Energy Convers. Manage.*, 1997, **38**, S37–S42, DOI: 10.1016/s0196-8904(96)00242-7.

10 R. H. Niswander, D. J. Edwards, M. S. DuPart and J. P. Tse, A more energy efficient product for carbon dioxide separation, *Sep. Sci. Technol.*, 1993, **28**, 565–578, DOI: 10.1080/01496399308019507.

11 A. Veawab, P. Tontiwachwuthikul and A. Chakma, Corrosion behavior of carbon steel in the CO_2 absorption process using aqueous amine solutions, *Ind. Eng. Chem. Res.*, 1999, **38**, 3917–3924, DOI: 10.1021/ie9901630.

12 J. P. H. Fee, J. M. Murray and S. R. Luney, Molecular sieves: an alternative method of carbon dioxide removal which does not generate compound A during simulated low-flow sevoflurane anaesthesia, *Anaesthesia*, 1995, **50**, 841–845, DOI: 10.1111/j.1365-2044.1995.tb05847.x.

13 G. Pannocchia, M. Puccini, A. Maurizia Seggiani and S. Vitolo, Experimental and modeling studies on high-temperature capture of CO_2 using lithium zirconate based sorbents, *Ind. Eng. Chem. Res.*, 2007, **46**, 6696–6706, DOI: 10.1021/ie0616949.

14 D. J. Fauth, E. A. Frommell, J. S. Hoffman, R. P. Reasbeck and H. W. Pennline, Eutectic salt promoted lithium zirconate: novel high temperature sorbent for CO_2 capture, *Fuel Process. Technol.*, 2005, **86**, 1503–1521, DOI: 10.1016/j.fuproc.2005.01.012.

15 J. Ida, R. Xiong and Y. S. Lin, Synthesis and CO_2 sorption properties of pure and modified lithium zirconate, *Sep. Purif. Technol.*, 2004, **36**, 41–51, DOI: 10.1016/S1383-5866(03)00151-5.

16 M. Kato, S. Yoshikawa and K. Nakagawa, Carbon dioxide absorption by lithium orthosilicate in a wide range of temperature and carbon dioxide concentrations, *J. Mater. Sci. Lett.*, 2002, **21**, 485–487, DOI: 10.1023/A:1015338808533.

17 K. Nakagawa and T. Ohashi, A novel method of CO_2 capture from high temperature gases, *J. Electrochem. Soc.*, 1998, **145**, 1344–1346, DOI: 10.1149/1.1838462.

18 B. N. Nair, R. P. Burwood, V. J. Goh, K. Nakagawa and T. Yamaguchi, Lithium based ceramic materials and membranes for high temperature CO_2 separation, *Prog. Mater. Sci.*, 2009, **54**, 511–541, DOI: 10.1016/j.pmatsci.2009.01.002.

19 S. C. Lee, H. J. Chae, S. J. Lee, B. Y. Choi, C. K. Yi, J. B. Lee, C. K. Ryu and J. C. Kim, Development of regenerable MgO-based sorbent promoted with K_2CO_3 for CO_2 capture at low temperatures, *Environ. Sci. Technol.*, 2008, **42**, 2736–2741, DOI: 10.1021/es702693c.

20 S. C. Lee, B. Y. Choi, S. J. Lee, S. Y. Jung, C. K. Ryu and J. C. Kim, CO_2 absorption and regeneration using Na and K based sorbents, *Stud. Surf. Sci. Catal.*, 2004, **153**, 527–530, DOI: 10.1016/S0167-2991(04)80307-0.

21 S. C. Lee, B. Y. Choi, T. J. Lee, C. K. Ryu, Y. S. Ahn and J. C. Kim, CO_2 absorption and regeneration of alkali metal-based solid sorbents, *Catal. Today*, 2006, **111**, 385–390, DOI: 10.1016/j.cattod.2005.10.051.

22 S. C. Lee and J. C. Kim, Dry potassium-based sorbents for CO_2 capture, *Catal. Surv. Asia*, 2007, **11**, 171–185, DOI: 10.1007/s10563-007-9035-z.

23 S. C. Lee, H. J. Chae, S. J. Lee, Y. H. Park, C. K. Ryu, C. K. Yi and J. C. Kim, Novel regenerable potassium-based dry sorbents for CO_2 capture at low temperatures, *J. Mol. Catal. B: Enzym.*, 2009, **56**, 179–184, DOI: 10.1016/j.molcatb.2008.07.007.

24 J. B. Lee, C. K. Ryu, J. I. Baek, J. H. Lee, T. H. Eom and S. H. Kim, Sodium-based dry regenerable sorbent for carbon dioxide capture from power plant flue gas, *Ind. Eng. Chem. Res.*, 2008, **47**, 4465–4472, DOI: 10.1021/ie0709638.

25 S. C. Lee, H. J. Chae, Y. M. Kwon, W. S. Lee, H. S. Nam, S. Y. Jung, J. B. Lee, C. K. Ryu and J. C. Kim, Characteristics of new potassium-based sorbents prepared with nano-titanium oxide for carbon dioxide capture, *J. Nanoelectron. Optoelectron.*, 2010, **5**, 212–217, DOI: 10.1166/jno.2010.1096.

26 C. Zhao, X. Chen, C. Zhao and Y. Liu, CO_2 absorption using dry potassium-based sorbents with different supports, *Energy Fuels*, 2009, **23**, 4683–4687, DOI: 10.1021/ef900182d.

27 C. Zhao, X. Chen and C. Zhao, Carbonation behavior of K_2CO_3 with different microstructure used as an active component of dry sorbents for CO_2 capture, *Ind. Eng. Chem. Res.*, 2010, **49**, 12212–12216, DOI: 10.1021/ie1018035.

28 C. Zhao, X. Chen and C. Zhao, K_2CO_3/Al_2O_3 for capturing CO_2 in flue gas from power plants. Part 1: Carbonation behaviors of K_2CO_3/Al_2O_3, *Energy Fuels*, 2012, **26**, 1401–1405, DOI: 10.1021/ef200725z.

29 W. Dong, X. Chen and Y. Wu, TiO_2-doped K_2CO_3/Al_2O_3 sorbents for CO_2 capture, *Energy Fuels*, 2014, **28**, 3310–3316, DOI: 10.1021/ef500133e.

30 S. Hirano, N. Shigemoto, S. Yamada and H. Hayashi, Fixed-Bed Operations over K_2CO_3-on-Carbon for the Recovery of Carbon Dioxide under Moist Conditions, *Bull. Chem. Soc. Jpn.*, 1995, **68**, 1030–1035, DOI: 10.1246/bcsj.68.1030.

31 H. Hayashi, J. Taniuchi, N. Furuyashiki, S. Sugiyama, S. Hirano, N. Shigemoto and T. Nonaka, Efficient recovery of carbon dioxide from flue gases of coal-fired power plants by cyclic fixed-bed operations over K_2CO_3-on-carbon, *Ind. Eng. Chem. Res.*, 1998, **37**, 185–191, DOI: 10.1021/ie9704455.

32 A. Gomez, A. Jayakumar and N. Mahinpey, Experimental verification of the reaction mechanism of solid K_2CO_3 during postcombustion CO_2 capture, *Ind. Eng. Chem. Res.*, 2016, **55**, 11022–11028, DOI: 10.1021/acs.iecr.6b02916.

33 Y. Duan, B. Zhang, C. S. Dan and J. K. Johnson, CO_2 capture properties of M–C–O–H (M = Li, Na, K) systems: a combined density functional theory and lattice phonon dynamics study, *J. Solid State Chem.*, 2011, **184**, 304–311, DOI: 10.1016/j.jssc.2010.12.005.

34 H. Gao, S. Pishney and M. J. Janik, First principles study on the adsorption of CO_2 and H_2O on the K_2CO_3(001) surface, *Surf. Sci.*, 2013, **609**, 140–146, DOI: 10.1016/j.susc.2012.11.014.

35 C. Zhao, X. Chen and C. Zhao, Effect of crystal structure on CO_2 capture characteristics of dry potassium-based sorbents, *Chemosphere*, 2009, **75**, 1401–1404, DOI: 10.1016/j.chemosphere.2009.02.045.

36 A. Jayakumar, A. Gomez and N. Mahinpey, Post-combustion CO_2 capture using solid K_2CO_3: Discovering the carbonation reaction mechanism, *Appl. Energy*, 2016, **179**, 531–543, DOI: 10.1016/j.apenergy.2016.06.149.

37 E. J. Karlsen, M. A. Nygren and L. G. M. Pettersson, Comparative study on structures and energetics of NO_x, SO_x, and CO_x adsorption on alkaline-earth-metal oxides, *J. Phys. Chem. B*, 2003, **107**, 7795–7802, DOI: 10.1021/jp0346716.

38 W. F. Schneider, Qualitative differences in the adsorption chemistry of acidic (CO_2, SO_x) and amphiphilic (NO_x) species on the alkaline earth oxides, *J. Phys. Chem. B*, 2004, **108**, 273–282, DOI: 10.1021/jp036323+.

39 J. K. Norskov and C. H. Christensen, Chemistry: Toward efficient hydrogen production at surfaces, *Science*, 2006, **312**, 1322–1323, DOI: 10.1126/science.1127180.

40 M. D. Segall, P. J. D. Lindan, M. J. Probert, C. J. Pickard, P. J. Hasnip, S. J. Clark and M. C. Payne, First-principles simulation: ideas, illustrations and the CASTEP code, *J. Phys.: Condens. Matter*, 2002, **14**, 2717, DOI: 10.1088/0953-8984/14/11/301.

41 S. Kurth, J. P. Perdew and P. Blaha, Molecular and solid-state tests of density functional approximations: LSD, GGAs, and meta-GGAs, *Int. J. Quantum Chem.*, 1999, **75**, 889–909, DOI: 10.1002/(SICI)1097-461X(1999)75:4/5<889::AID-QUA54>3.0.CO;2-8.

42 S. Grimme, S. Ehrlich and L. Goerigk, Effect of the damping function in dispersion corrected density functional theory, *J. Comput. Chem.*, 2011, **32**, 1456–1465, DOI: 10.1002/jcc.21759.

43 W. Zhang, C. Chen and S. Zhang, Equilibrium crystal shape of Ni from first principles, *J. Phys. Chem.*, 2013, **41**, 21274–21280, DOI: 10.1021/jp404569m.

44 Y. Idemoto, J. W. Richardson and N. Koura, Crystal structure of $(Li_xK_{1-x})_2CO_3$ (x = 0, 0.43, 0.5, 0.62, 1) by neutron powder diffraction analysis, *J. Phys. Chem. Solids*, 1998, **59**, 363–376, DOI: 10.1016/S0022-3697(97)00209-6.

45 C. Zhao, X. Chen, C. Zhao and Y. Liu, Carbonation and hydration characteristics of dry potassium-based sorbents for CO_2 capture, *Energy Fuels*, 2009, **23**, 1766–1769, DOI: 10.1021/ef800889m.

46 C. Zhao, X. Chen and C. Zhao, Carbonation Behavior and the Reaction Kinetic of a New Dry Potassium-Based Sorbent for CO_2 Capture, *Ind. Eng. Chem. Res.*, 2012, **51**, 14361–14366, DOI: 10.1021/ie302497r.

47 D. C. Sorescu, J. Lee, W. A. Al-Saidi and K. D. Jordan, Coadsorption properties of CO_2 and H_2O on TiO_2 rutile (110): a dispersion-corrected DFT study, *J. Chem. Phys.*, 2012, **137**, 074704, DOI: 10.1063/1.4739088.

